

Electride properties of ternary silicide and germanide of La and Ce

Alexey A. Dyachenko ^{1,2,*}, Alexey V. Lukoyanov ^{1,2,3}, Vladimir I. Anisimov ^{1,2,3} and Artem R. Oganov ²

¹*M. N. Mikheev Institute of Metal Physics of Ural Branch of Russian Academy of Sciences, Yekaterinburg 620108, Russia*

²*Skolkovo Institute of Science and Technology, Moscow 121205, Russia*

³*Institute of Physics and Technology, Ural Federal University, Yekaterinburg 620002, Russia*



(Received 5 August 2020; revised 18 November 2021; accepted 31 January 2022; published 24 February 2022)

We present a theoretical study of the electronic, spectral, and magnetic properties of ternary $REScSi$ and $REScGe$ ($RE = La, Ce$) compounds based on the DFT+DMFT method combining Density Functional Theory with Dynamical Mean-Field Theory. In this work, we find that Ce-based compounds, similar to $LaScSi$, exhibit electride-like features. Our calculations reveal that not only silicide $REScSi$ compounds, but also their germanide $REScGe$ analogs, exhibit high interstitial density characteristic of electrified. Remarkably, we find that both rare-earth $5d$ and scandium $3d$ contribute electrons to the strongly localized interstitial electron density, which can be considered as an electride anion with pronounced s symmetry. In addition, we show that the Ce-based compounds show effects of strong electronic correlations in the $4f$ shell of cerium ions and strongly resemble those of γ -Ce.

DOI: [10.1103/PhysRevB.105.085146](https://doi.org/10.1103/PhysRevB.105.085146)

I. INTRODUCTION

Electrides are a class of materials in which some electrons, localized within the crystal voids, act as anions [1–13]. In recent years, their unique properties derived from the high anionic electron density and low binding energies attracted great scientific interest. However, theoretical studies of these properties remain relatively few. In this work, we use approaches based on density functional theory (DFT) and dynamical mean-field theory (DMFT) to investigate the electronic structure and magnetic properties of ternary silicides and germanides of La and Ce ($LaScSi$, $CeScSi$, $LaScGe$, and $CeScGe$) at room temperature.

In electrifieds, some valence electrons, which are localized in the interstitial regions of a crystal, often experience weak binding and serve as electron anions. Such electrons cause unique electronic and magnetic properties of electrifieds [5,10,14–16], such as an extremely low work function and strong reducing character [4,17]. The first electride properties were observed in the alkali metal-doped crown ether ($Cs^+(18C6):e^-$) [8]. However, organic electrifieds are unstable above room temperature and chemically sensitive to air and moisture, which greatly limit their potential applications. The discovery of an inorganic electride [$Ca_{24}Al_{28}O_{64}$]⁴⁺(e^-)₄ ($C12A7:e^-$) [10], which was successfully applied as a promoter of Ru in the catalytic synthesis of ammonia, has greatly stimulated studies of electride materials. The exotic chemical and physical properties of electrifieds are important for catalysis, chemical synthesis, and optoelectronics [18–21].

Rare-earth (RE) scandium silicon and germanium intermetallics $REScSi$ and $REScGe$ ($RE = Ce, La$) crystallize in a tetragonal La_2Sb structure type with space group $I4/mmm$

[22–24]. Cerium and lanthanum ternary compounds absorb hydrogen in tetrahedral RE_4 sites when exposed to hydrogen gas at 3–4 MPa and 523 K, which alters their chemical, magnetic, and structural properties [25–32]. For example, upon hydrogenation, tetragonal $CeFeSi$ -type compounds $CeCoSi$, $CeCoGe$, and $CeRuSi$ adopt the $ZrCuSiAs$ structure, with an increase in the unit cell volume and the formation of Ce–H bonding. Similarly, it has been shown for $REScSi$ and $REScGe$ ($RE = La, Ce$) that the insertion of hydrogen leads to an expansion of the cell, Kondo behavior of the resistivity, and a decrease in the magnetic ordering temperature [24].

A recent study has shown that $LaScSi$, one of the rare-earth intermetallic compounds, exhibits electride properties because of its crystal voids accommodating anionic electrons, and has a very high catalytic activity in the Ru-based ammonia synthesis [33]. Theoretical and experimental studies of the hydrogenation of $LaScSi$ and its catalytic and electride properties have shown that the exposure of this compound to hydrogen gas at 260–400°C results in the formation of $LaScSiH_{1.5}$ without any crystal structure transition. It has been shown that the hydrogen atoms occupy two voids in $LaScSi$: one in the La_4 tetrahedra and the other in the La_2Sc_4 octahedra. While the charge density calculations show that initially only the La_4 void has an excess of electron density and is susceptible to the hydrogen absorption, it has been reported that only after the hydrogenation to $LaScSiH$, the La_2Sc_4 void starts to exhibit anionic character. Further hydrogenation leads to the occupation of the void by the hydrogen atom and the final composition is $LaScSiH_{1.5}$.

While the catalytic and electride properties of $LaScSi$ have attracted experimental and theoretical attention, $CeScSi$ and the germanide analogs of these compounds remain unexplored, and without sufficient amount of data to determine their potential electride-like character. Unlike $LaScSi$ with its empty $5d$ and $4f$ shells, the cerium atoms in $CeScSi$

*dyachenko@imp.uran.ru

should exhibit strong electronic correlations. Cerium metal has a very rich physics that depends on the interplay between the Coulomb interaction, spin-orbit coupling, and crystal field splitting. Under pressure, Ce undergoes the isostructural α - γ phase transition with a 15% volume collapse [34]. To describe the bulk properties and equation of state of Ce, various theoretical methods have been applied, among them DFT [35,36], DFT+GW [37–39], RPA [40], and others. Today, the approach combining density functional theory and dynamical mean-field theory (DFT+DMFT) is one of the most successful methods to correctly describe the magnetic state and reproduce the spin, metal-insulator, and structural transitions under pressure in compounds with strong correlations, in particular, Ce and its compounds [41–43]. This approach, accounting for the dynamic effects and strong electronic correlations, has been used in studies of many transition metal compounds such as MnO [44], (Mg, Fe)O [45], MnSe [46], BiFeO₃ [47], CoO [48], Fe₂O₃ [49], FeSiO₃ [50], and FeS [51]. It was successful in investigations of the α - γ phases of cerium [52–59], Ce-115 materials (CeRhIn₅, CeCoIn₅, and CeIrIn₅), Ce pnictides (CeN, CeP, CeAs, CeSb, CeBi) [60], and Ce-122 ternary compounds (CeM₂Si₂, where $M = \text{Ru, Rh, Pd}$) [61,62].

In this work, we combine the DFT and DFT+DMFT approaches to investigate the electronic structure and electrone properties of rare-earth silicide and germanide ternary compounds $RE\text{ScSi}$ and $RE\text{ScGe}$ ($RE = \text{La, Ce}$).

II. METHODS

Our computational scheme of the DFT+DMFT method [42] starts with the self-consistent DFT calculations. Using the generalized gradient approximation [63] implemented in ELK package [64], we produced a noninteracting Hamiltonian, then set up a many-body Hamiltonian, and finally, the DMFT equations for this Hamiltonian were solved self-consistently. For the Sc-3*d*, RE-5*d*, 4*f*, Si-3*p*, and Ge-4*p* orbitals, we constructed a basis set of Wannier functions [65,66] employing the projection procedure described in detail in Ref. [67]. All bands of the basis set formed by the chosen states were included and projected on the Bloch functions for these bands.

The interaction matrix for the quantum impurity model was parameterized by the values of the Coulomb repulsion parameter U and Hund exchange parameter J_{H} in the density-density approximation. The interaction parameters were calculated using the constrained random phase approximation (cRPA) method; for Sc-3*d*, the Coulomb repulsion parameter $U = 1.7$ eV, the Hund parameter $J_{\text{H}} = 0.8$ eV. For Ce, $U = 2.0$ eV and $J_{\text{H}} = 0.5$ eV. The calculated Coulomb interaction parameter for Ce-4*f* was smaller than 6.0 [57–59,68] and 5.5 eV [69], the values obtained using constrained DFT for elemental Ce; it was close to 2.5 eV derived from the hybrid functional results [70]. However, it is known for cRPA to underestimate the interaction parameter for γ -Ce when calculated without specific treatment [71], and thus we used $U = 6.0$ eV for cerium impurities throughout this work; the same parameter was used for La-4*f* impurities. The Hund parameter was in the ballpark of the values commonly taken in the literature as 0.0 [57,58,68] or 0.7 eV [59], or calculated as 0.58 eV [69]. Finally, the cRPA calculations for the rare-earth 5*d*

states yielded the Coulomb interaction parameter of only about 0.5 eV; therefore these states were treated as uncorrelated in the DFT+DMFT calculations. The DFT+DMFT problem was solved in a fully charge self-consistent manner. We used the fully localized limit scheme for double-counting correction [72]. The continuous-time quantum Monte Carlo hybridization-expansion solver from AMULET package [73] was employed to solve the effective DMFT quantum impurity problem [74]. Some code from the ALPS Project was used for the calculations [75]. The presented spectral functions were calculated from the real frequency lattice Green's functions $G(\omega)$ using the Páde approximants [76] for the analytical continuation to the real energy axis, as implemented in AMULET package. The maximally localized Wannier functions of $RE\text{ScSi}$ and $RE\text{ScGe}$ ($RE = \text{La, Ce}$) were calculated with WANNIER90 program [77] using QUANTUM ESPRESSO suite [78]. Bader [79] charges were calculated using BADER code [80]. Crystal structures and electron localization functions were visualized using VESTA program [81]. See the Supplemental Material [82] for computational details.

III. RESULTS AND DISCUSSION

A. Electron localization function

First, we performed the ground-state DFT calculations using the experimental crystal structures of $RE\text{ScSi}$ and $RE\text{ScGe}$ ($RE = \text{Ce, La}$) from Ref. [24]. To investigate the localization of the anion electrons in the voids of these intermetallics, we calculated the electron localization function (ELF) of these compounds. A 2D slice ([201] plane) of the ELF of LaScSi plotted along both hydrogen positions is shown in Fig. 1(a). Throughout the work, we will refer to the crystal void in La₄ tetrahedra as V_1 , to the void in La₂Sc₄ octahedra as V_2 , and to the remaining void in Sc plane as V_3 . Our calculations show a strong electron localization in V_2 , with the ELF of 0.87. On the other hand, in V_1 the ELF value is about 0.34, which is below the localization criterion of 0.5 [83]. Moderate amount of delocalized electrons between the La layers can be attributed to the metallic bonding between the La atoms. Thus, the LaScSi electrone can be formulated as $[\text{LaScSi}]^{0.5+}(e^-)_{0.5}$. The calculated results differ from the observations made in Ref. [33], where the electron density maps for nonhydrogenated LaScSi showed the presence of excess electrons in V_1 and no electrons in V_2 , and upon the hydrogenation V_1 has been occupied by a hydrogen atom, and V_2 has shown the presence of excess electrons.

The ELF isosurface in LaScSi, calculated from the interstitial part of the charge density, is shown in Fig. 1(c). In the Sc layer, the excess electrons are localized only in V_2 , in the voids between the nearest La atoms of the adjacent La layers. The remaining voids in the Sc layer exhibit no localization, with $\text{ELF} \approx 0.40$. Figure 1(b) shows a [001] plane ELF slice of the Sc layer of $RE\text{ScSi}$ and $RE\text{ScGe}$ ($RE = \text{La, Ce}$) intermetallics. For LaScSi and LaScGe, no difference is observed in the size of the electrone anion and the degree of localization, the ELF value in V_2 is ≈ 0.87 for both compounds. For the Ce-based compounds, the ELF of the electrone anion has a slightly lower volume and the values of 0.847 and 0.843 in V_2 for CeScSi and CeScGe, respectively. Peculiarly, the V_1 void

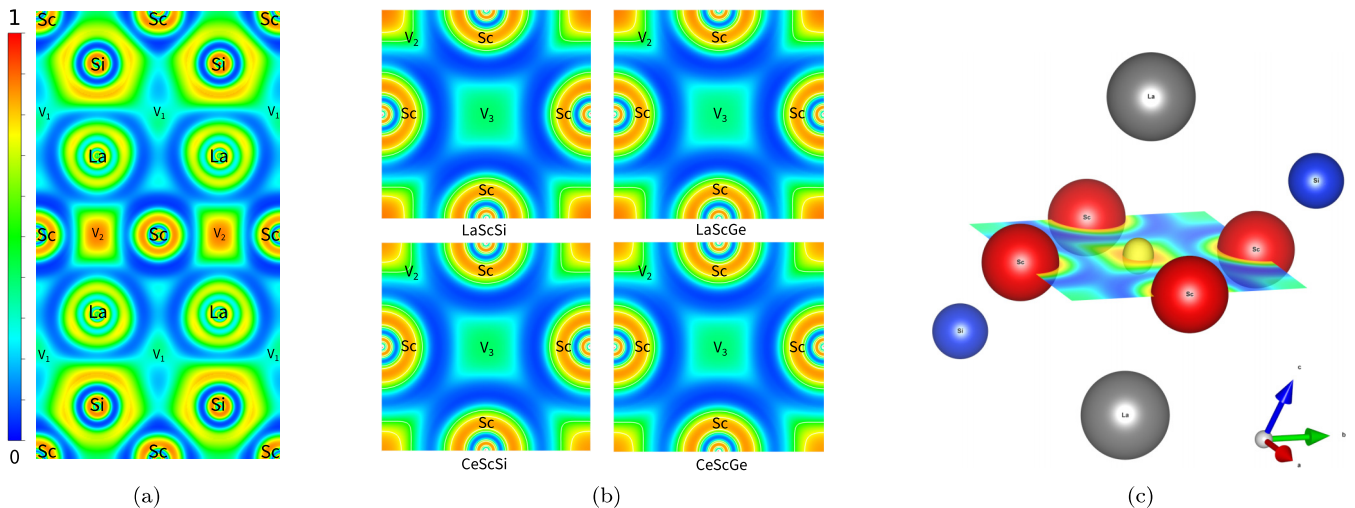


FIG. 1. (a) [201] plane electron localization function (ELF) slice of LaScSi along the possible hydrogen positions: V_1 in the La_4 tetrahedra and V_2 in the La_2Sc_4 octahedra. (b) [001] ELF slice of LaScSi, LaScGe, CeScSi, and CeScGe. (c) Interstitial-only ELF isosurface at level 0.85 of the LaScSi primitive cell (shifted by $[-0.5, -0.5, 0.0]$ for clarity).

in cerium compounds exhibits higher, than in LaScSi, electron localization with ELF value of ≈ 0.52 .

To evaluate the nature and origin of interstitial (IS) electrons in $REScSi$ and $REScGe$, we employed the maximally localized Wannier function (MLWF) projection procedure. Unlike the conventional DFT band structure and density of states, which are a projection of the Kohn-Sham eigenstates of atoms in the system, the MLWFs make it possible to project the electron density localized in atomic voids, which makes them a great tool for studies of electrider properties [16,84–87].

First, to ensure the consistency and validity of the MLWF projection, we constructed the MLWF for a set of atomic wave functions corresponding to the atomic orbitals in the system (Si- s, p , La- d, f , Sc- d) and compared the results of the projection procedure to those of the non-MLWF approach [67] that uses pseudoatomic orbitals as a set of trial orbitals for projection. The results of both methods are in close agreement. Next, we expanded the set of projection functions with an extra s -symmetry Wannier function (WF) centered at the electron anion in void V_2 . In contrast to the pseudoatomic projection, the initial choice of the WF symmetry and position is not unique, but the iterative MLWF projection procedure ensures the uniqueness of the WF position, shape, and spatial extent. In the usual Wannier projection procedure, the Kohn-Sham band structure in the chosen energy window gets downfolded onto a specified number of WF. However, the inclusion of an extra WF, which corresponds to the void-centered electron density, allows us to unfold the electronic states from its origin atom. After the iterative MLWF projection procedure, the interstitial WF remained centered at void V_2 and had a slightly distorted s symmetry [Fig. 2(a)]. A qualitative judgment about the origin of an excess electron density in V_2 can be made by comparing the resulting atomic and extended Hamiltonians. The densities of states (DOS) of WF from both sets of projections are shown in Fig. 2(b). Functionally, in our calculations, the largest difference in the WF density between two Wannier projections comes from the La- d states near the Fermi level. The calculated DOS of

the interstitial WF is in close agreement with the previously reported projected DOS of the interstitial states in V_2 obtained by Wu *et al.* [33] using the reversed approximation molecular orbital method. Interestingly, rare-earth elements and Sc have low electronegativities, which could be a key reason for the formation of excess electron density in the interstices.

The MLWF band structure with separate contributions from each group of the projected WF is shown in Fig. 3. The interstitial WF is localized mostly in two bands near the Fermi level, around Y, P, X, and Y_1 points of the Brillouin zone. Localization of electrider states near the Fermi level is one of the frequent (though not universal) characteristics of an electrider compound [88]. On the other hand, the La- $4f$ orbitals are localized in the narrow energy range from 1.8 to 3.0 eV, whereas the La- $5d$ orbitals are heavily overlapped with Sc- $3d$ orbitals, and are widely spread from -0.5 eV up to the projection window cutoff, together with some amount of $6s$ and $6p$ states at very high energies, which are present in the pseudopotentials and were naturally included in the projection because of downfolding. The bands of the Si- $3s$ and Si- $3p$ states are localized at -7.0 eV and in the range from -4.0 to 0.0 eV, respectively. However, at the Fermi level around Y, P, X, and Y_1 points, in the energy region of interest, mostly La- $5d$ and Sc- $3d$ localizations are observed. The calculated band contributions of the extra s -WF in the extended Hamiltonian suggest that the excess electron density, observed in the center of the La_2Sc_4 octahedra, is in large part associated with La- $5d$ and Sc- $3d$ states.

Usually, in the case of electrideres, the localized electron density in the voids of the crystal manifests as maximum in charge density. However, this is not the case for the inorganic electrider ($C12A7:e^-$) where there are no non-nuclear maxima in the charge density [88]. Although the charge density shows no maxima in the voids, other methods such as ELF have been successful in the description of localized electrons [89]. For the systems at hand, our Bader charge calculations reveal the presence of only one non-nuclear charge density maximum and the corresponding interstitial basin of attraction, which is located at V_2 and correlates with the shape of

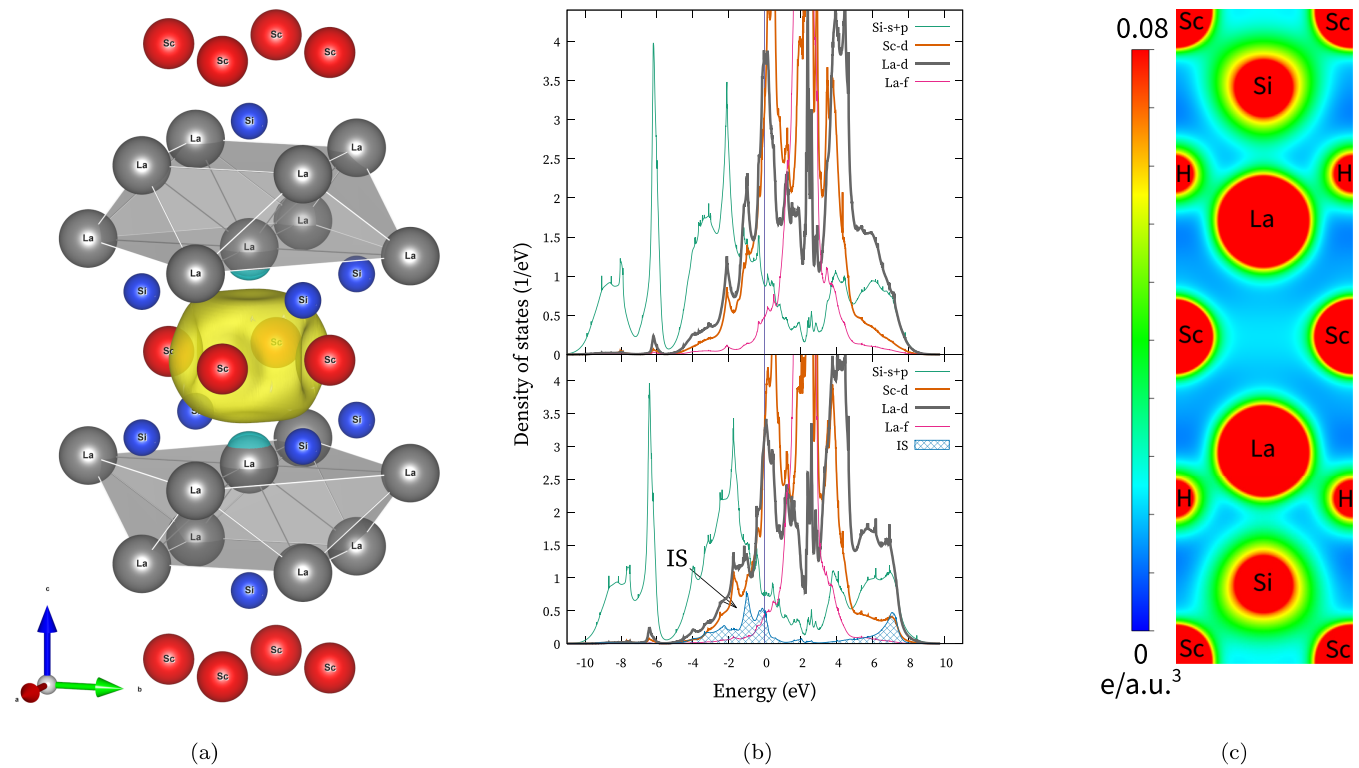


FIG. 2. (a) Maximally localized Wannier function (MLWF) projection of the interstitial density from the extended Hamiltonian of LaScSi. (b) DFT density of states of the atomic MLWF Hamiltonian (top) and extended Hamiltonian with an additional interstitial Wannier function (bottom). (c) [201] charge density slice of LaScSiH along V_1 (occupied by hydrogen) and V_2 . The cutoff is $0.08 e/a.u.^3$.

the high-localization ELF. However, the calculated charge of each basin (and there is one such basin per unit cell) is very low, 0.064 electrons (≈ 0.035 for Ce-based compounds), and the charge density maximum is very low at V_2 . We found

LaScSi to lack a non-nuclear maximum in V_1 , the lack of electrons in which is also supported by our ELF and Bader charge calculations. Additionally, our calculations show no charge density topology changes in V_2 with hydrogenation

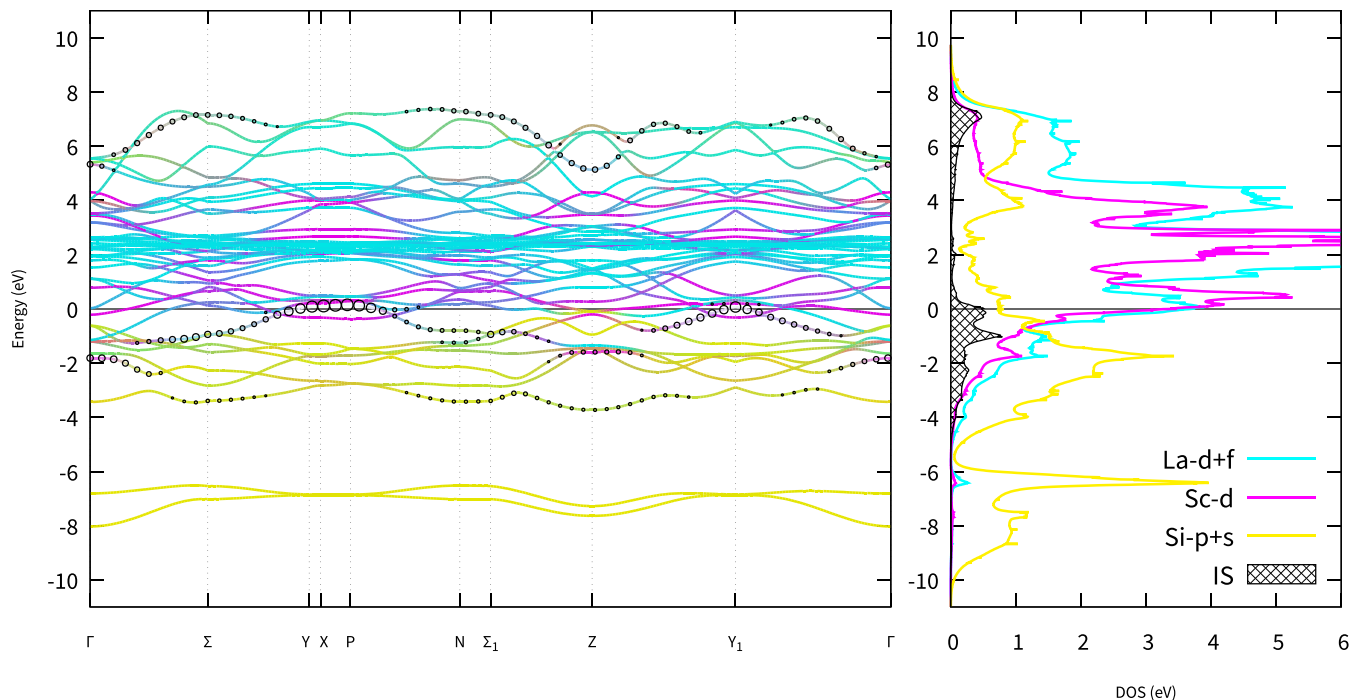


FIG. 3. MLWF band structure of LaScSi (left). The contributions of La- $d+f$, Sc- d , Si- $s+p$, are shown in color corresponding to the MLWF density of states (right) The interstitial density Wannier function is shown by the weighted circle symbols on the band structure.

of the system (H atoms in V_1) as described in Ref. [33]. The calculated charge density of LaScSiH is presented in Fig. 2(c), one can find the low electronic charge density in the region of high electron localization.

B. Electronic correlation effects

To investigate the influence of the electronic temperature and correlations on the electronic structure and magnetic properties of $REScSi$ and $REScGe$ ($RE = La, Ce$) and, in particular, on the electrider states, we carried out DFT+DMFT calculations at an electronic temperature of 300 K ($\beta = 38.6817 \text{ eV}^{-1}$). Because the chosen temperature is well above the Néel temperature T_N (which equals 26 and 43 K for CeScSi and CeScGe [24], respectively), our calculations resulted in the paramagnetic state for all compounds. In particular, because empty La-4*f* orbitals appear to be uncorrelated, the result is a low value of the local magnetic moment of the impurity $\sqrt{\langle \mu_z^2 \rangle} = 0.29 \mu_B$. For the Ce-4*f* quantum impurity, we observed a local magnetic moment $\sqrt{\langle \mu_z^2 \rangle} = 1.02 \mu_B$ with the occupancy of 1.04 electrons. Furthermore, our calculations have shown that Sc-*d* and La-*f*, unlike Ce-*f* impurities, appear to be uncorrelated, as one can expect. For Sc-*d* in all compounds, and for La-*d*, with Coulomb correlations, we observe a simple shift of unoccupied bands relative to the Fermi level, determined by a combination of the Coulomb correlation parameter and double counting. Consequently, we will focus mostly on cerium compounds further in this section, CeScSi, in particular, as its germanide counterpart is electronically analogous.

We present DFT+DMFT calculated spectral functions of CeScSi in Fig. 4. The obtained spectral functions of Ce-*f* greatly resemble those of β and γ phases of elemental cerium [59]. Taking into account crystal structures of CeScSi and allotropes of elemental cerium, the isostructural α and γ phases bear some structural similarity to the CeScSi: The silicide structure has two squashed along *z*-axis *fcc*-like layers of rare-earth atoms which are sandwiched between Sc-Si layers. Additionally, we do not observe a sharp Kondo resonance peak which is present in α -Ce. Firstly, the absence of Kondo resonance could be explained by the chosen temperature regime of 300 K, which is between regimes of β - and γ -Ce. The second factor is the greatly increased Ce-Ce distances, compared to γ -Ce and α -Ce. The possibility of the Kondo resonance effect in CeScSi is of interest for further investigations. Given the absence of a sharp Kondo resonance peak in the vicinity of Fermi level, which is greatly affected by the spin-orbit coupling in α -Ce [59], we have chosen to neglect the effect of the spin-orbit correction in our calculations.

The calculated CeScSi DFT+DMFT spectra show two pronounced Hubbard bands at -3.8 and 3.5 eV. Compared to elemental cerium, the Hubbard bands in CeScSi are located lower by about 1 eV, which is due to the presence of Sc and Si states in the vicinity of the Fermi level. The exception, however, is two degenerate orbitals with the occupation number of 0.013 electrons (versus 0.05–0.14 of the rest of the orbitals) which do not have enough occupancy to form the lower Hubbard band (we provided partial Ce-*f* spectral functions in the Supplemental Material [82]). The DFT+DMFT configuration weights show domination of $4f^1$ configuration with a weight

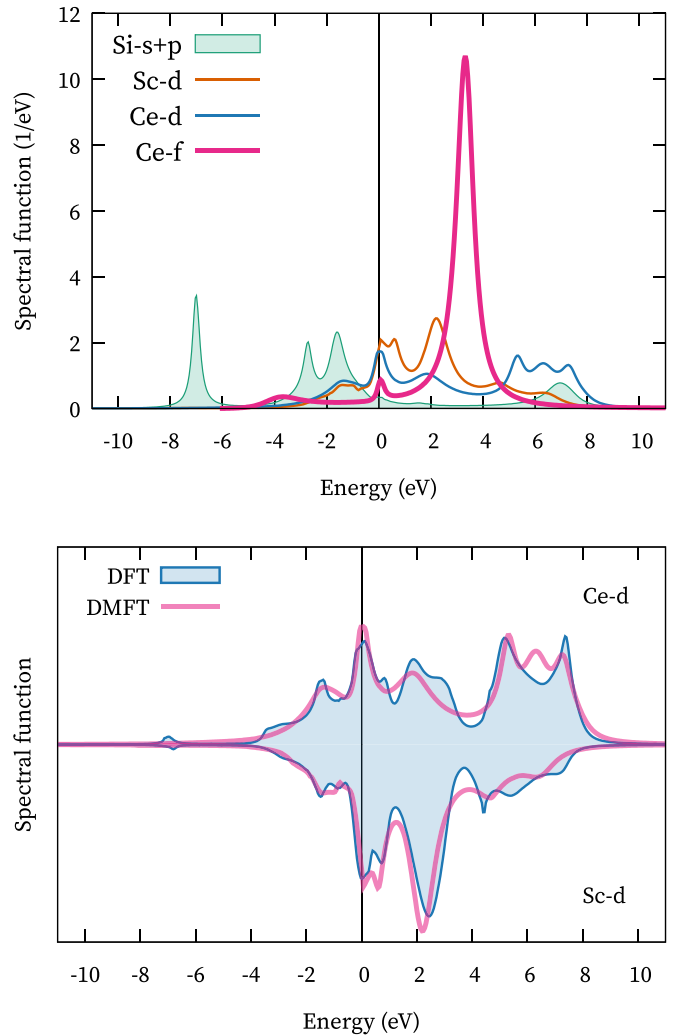


FIG. 4. (Top) DMFT spectral functions of CeScSi compound. (Bottom) Spectral functions of the interstitial density bearing Ce-*d* (up) and Sc-*d* (down) Wannier functions computed within DFT and DMFT methods.

of 95%, whereas $4f^2$ and $4f^0$ have weights of 4% and 1%, respectively. The high $4f^1$ configuration probability is indicative of a well-localized state of 4*f* electrons and of suppressed hybridization with *spd* electrons, similar to β , γ , and δ phases of cerium that do not exhibit Kondo resonance peak due to weaker hybridization with *spd* electrons.

The state of the electrider electron in the DMFT calculations is of particular concern. Our MLWF projections for the electrider electron show a great contribution from Sc-*d* and RE-*d* states. In Fig. 4, we show uncorrelated Sc-*d* and Ce-*d* WF spectral functions and the corresponding DMFT results. While Sc-*d* and RE-*d* states in our case exhibit little to no correlations, it is possible for an electrider electron to be strongly correlated. Between these two, Sc-*d* has the largest calculated Coulomb interaction parameter of 1.7 eV, which can potentially lead to a pretty high value of Coulomb parameter for standalone electrider *s* orbital. However, while the Coulomb correlation strength can be estimated for both RE-*d* and Sc-*d*, it is difficult to calculate the U for the electrider MLWF s

orbital. Thus, we consider the density renormalization due to strong correlations in the Ce-*f* to have the greatest effect on electrone electrons in our investigation.

It is interesting to investigate the effect of DMFT density renormalization on the localization of the electrone anion. To that end, we consider DMFT density renormalization in the calculation of the ELF. Conventional ELF $\eta(r)$ is calculated as follows:

$$\eta(r) = \frac{1}{1 + (D/D_h)^2}, \quad (1)$$

where D , a measure of electron localization, is being compared to corresponding value for a uniform electron gas D_h :

$$D = \frac{1}{2} \sum_{i=1}^N |\nabla \psi_i|^2 - \frac{1}{8} \frac{|\nabla \rho|^2}{\rho}, \quad (2)$$

$$D_h = \frac{3}{10} (3\pi^2)^{2/3} \rho^{5/3}, \quad (3)$$

$$\rho(r) = \sum_{k\nu} f(\varepsilon_{k\nu}) \langle r | \Psi_{\nu k} \rangle \langle \Psi_{\nu k} | r \rangle. \quad (4)$$

In the case of a fully charge self-consistent calculation, the charge density $\rho(r)$, its gradients, and its wave-function gradients, instead of the diagonal Fermi function $f(\varepsilon_{k\nu})$ also contain nondiagonal correlation-induced density correction $N_{\nu\nu'}^{fscf}(\mathbf{k}) = f(\varepsilon_{k\nu})\delta_{\nu\nu'} + \Delta N_{\nu\nu'}(\mathbf{k})$. Having incorporated DMFT density correction into the cycle, the next step we can take is to plot partial ELF—an electron localization function that corresponds to a set of Wannier functions. To that end, we transform $N_{\nu\nu'}^{fscf}(\mathbf{k})$ to WF basis, zero all other WF, and then transform the matrix back to KS basis. Afterward, we use the obtained occupation matrix in the ELF calculation to obtain a function corresponding to a selected set of WFs.

In Fig. 5, we show interstitial-only ELF plots for Ce-*d* and Sc-*d* WFs in the plane along both Ce₂Sc₄ octahedra and Ce₄ tetrahedra (plane [110] that intersects both V₁ and V₂ and none of the atoms). Partial ELF isosurface plots for all WFs of CeScSi, along with contour plots for comparison between DFT and DFT+DMFT ELF, are presented in the Supplemental Material [82]. Bear in mind that in the case of partial density ELF calculation, the absolute ELF value is less useful and localization criteria of ELF >0.5 cannot be applied here; however, partial ELF can tell us about contribution ratios of different atoms to the sites of interstitial electron localization. As we have chosen most of the relevant states for the Wannier basis, the ELF plot of the full Wannier basis qualitatively appears to be the same as the one computed from the full charge density. The ELF plot indicates that most of the interstitial contribution from Ce-*d* WF localizes in V₁, while the contribution to V₂ is weaker. In V₁ the full DFT+DMFT ELF value is about 0.50 (slightly down from the pure DFT result of 0.52). On the other hand, the partial ELF plot of Sc-*d* states indicates that Sc-*d* WFs contribute only to the interstitial electron in V₂. Taking both results into account, we can conclude that the delocalized electron density in V₁ void stems mainly from Ce-*d*, while the highly localized electrone anion in V₂ is associated with both Ce-*d*, and, to a greater extent, with Sc-*d* states.

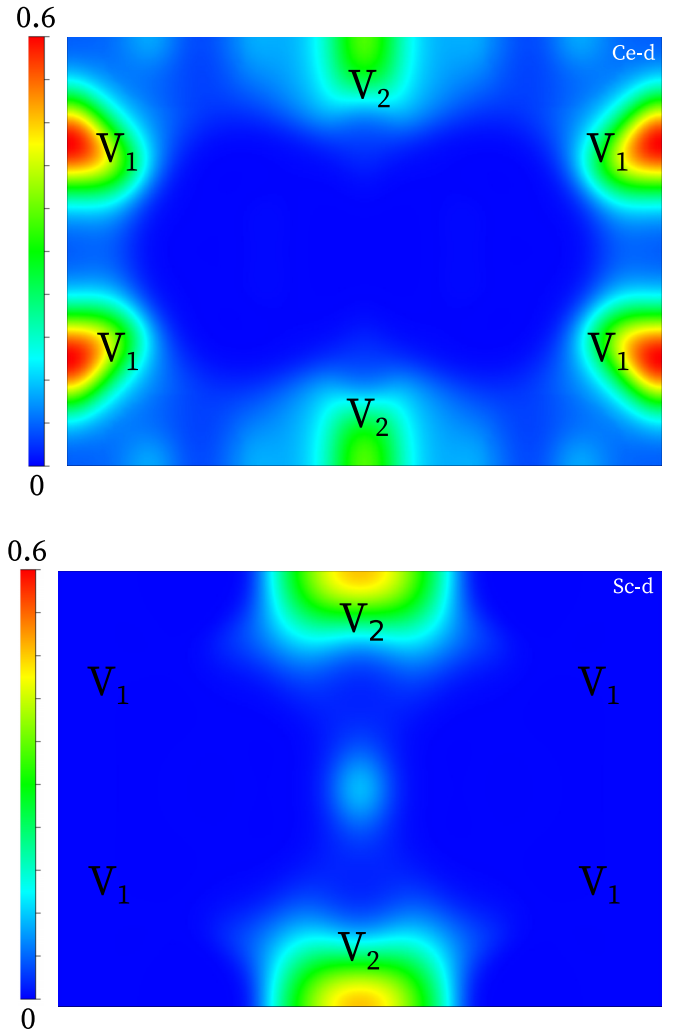


FIG. 5. DFT+DMFT interstitial-only partial ELF of CeScSi (plane [110], along both V₁ and V₂ voids). (Top) Partial ELF for Ce-*d* WFs. (Bottom) Partial ELF for Sc-*d* WFs.

IV. CONCLUSIONS

We studied the electronic, spectral, and magnetic properties of the REScSi and REScGe rare-earth compounds (RE = La, Ce) using the DFT+DMFT method. Our calculations show a strong electron localization in the crystal voids (RE₂Sc₄ octahedra) in both cerium and lanthanum ternary compounds. While the substitution of the La atom for the Ce atom only slightly decreases the size of the electrone anion, our results show no difference in interstitial electron density between Si and Ge counterpart compounds. Employing the maximally localized Wannier function projection, we conclude that both rare-earth 5*d* and scandium 3*d* orbitals contribute to the RE₂Sc₄ octahedra electrone electron in [REScSi]^{0.5+}(e⁻)_{0.5} and [REScGe]^{0.5+}(e⁻)_{0.5} electrines. The obtained Wannier-projected band structure and density of states demonstrate interstitial electronic states to be near the Fermi level. The other possible hydrogen location—the RE₄ tetrahedra—shows only a small amount of delocalized electrons, which are formed, as shown by the Wannier-projected

partial electron localization functions, by the rare-earth $5d$ states. On the other hand, the partial electron localization functions allowed us to estimate the degree of electron contribution to RE_2Sc_4 octahedra, where the influence of $Sc-3d$ states appears to be stronger. While the electron localization degree in RE_2Sc_4 octahedra is similar for both cerium and lanthanum compounds, the cerium compounds show a higher degree of localization in RE_4 tetrahedra. Our DFT+DMFT calculations show little effect of the electronic correlations for the La-based compounds. In contrast, CeScSi and CeScGe exhibit a strong renormalization of the electron density due to strong electronic correlations in the Ce- $4f$ shell, which cause

the formation of the Hubbard bands in the narrow localized $4f$ orbitals.

ACKNOWLEDGMENTS

The results in Sec. III A were obtained within the state assignment of the Ministry of Science and Higher Education of the Russian Federation (theme “Electron” No. AAAA-A18-118020190098-5). The results in Sec. III B were obtained within the grant of the Russian Science Foundation (Project No. 19-72-30043). A.A.D. acknowledges IMP Young Researchers Grant No. m25-21.

-
- [1] D. Issa and J. L. Dye, Synthesis of cesium 18-crown-6: The first single-crystal electride? *J. Am. Chem. Soc.* **104**, 3781 (1982).
- [2] R. H. Huang, M. K. Faber, K. J. Moeggenborg, D. L. Ward, and J. L. Dye, Structure of k^+ (cryptand[2.2.2]) electride and evidence for trapped electron pairs, *Nature (London)* **331**, 599 (1988).
- [3] J. L. Dye, Electrides: Early examples of quantum confinement, *Acc. Chem. Res.* **42**, 1564 (2009).
- [4] D. J. Singh, H. Krakauer, C. Haas, and W. E. Pickett, Theoretical determination that electrons act as anions in the electride $cs^+(15\text{-crown-5})_2 \cdot e^-$, *Nature (London)* **365**, 39 (1993).
- [5] K. Lee, S. W. Kim, Y. Toda, S. Matsuishi, and H. Hosono, Dicalcium nitride as a two-dimensional electride with an anionic electron layer, *Nature (London)* **494**, 336 (2013).
- [6] J. L. Dye, Electrons as anions, *Science* **301**, 607 (2003).
- [7] J. L. Dye, Electrides: Ionic salts with electrons as the anions, *Science* **247**, 663 (1990).
- [8] A. Ellaboudy, J. L. Dye, and P. B. Smith, Cesium 18-crown-6 compounds: A crystalline ceside and a crystalline electride, *J. Am. Chem. Soc.* **105**, 6490 (1983).
- [9] P. V. Sushko, A. L. Shluger, K. Hayashi, M. Hirano, and H. Hosono, Electron Localization and a Confined Electron Gas in Nanoporous Inorganic Electrides, *Phys. Rev. Lett.* **91**, 126401 (2003).
- [10] S. Matsuishi, Y. Toda, M. Miyakawa, K. Hayashi, T. Kamiya, M. Hirano, I. Tanaka, and H. Hosono, High-density electron anions in a nanoporous single crystal: $[Ca_{24}Al_{28}O_{64}]^{4+}(4e^-)$, *Science* **301**, 626 (2003).
- [11] D. L. Dexter, Note on the absorption spectra of pure and colored alkali halide crystals, *Phys. Rev.* **83**, 435 (1951).
- [12] F. Karsai, P. Tiwald, R. Laskowski, F. Tran, D. Koller, S. Gräfe, J. Burgdörfer, L. Wirtz, and P. Blaha, F center in lithium fluoride revisited: Comparison of solid-state physics and quantum-chemistry approaches, *Phys. Rev. B* **89**, 125429 (2014).
- [13] J. L. Dye, Electrides: From 1d Heisenberg chains to 2d pseudometals, *Inorg. Chem.* **36**, 3816 (1997).
- [14] A. Walsh and D. O. Scanlon, Electron excess in alkaline earth sub-nitrides: 2d electron gas or 3d electride? *J. Mater. Chem. C* **1**, 3525 (2013).
- [15] M.-S. Miao and R. Hoffmann, High pressure electrides: A predictive chemical and physical theory, *Acc. Chem. Res.* **47**, 1311 (2014).
- [16] M.-S. Miao, R. Hoffmann, J. Botana, I. I. Naumov, and R. J. Hemley, Quasimolecules in compressed lithium, *Angew. Chem., Int. Ed.* **56**, 972 (2017).
- [17] Y. Toda, H. Yanagi, E. Ikenaga, J. Kim, M. Kobata, S. Ueda, T. Kamiya, M. Hirano, K. Kobayashi, and H. Hosono, Work function of a room-temperature, stable electride $[Ca_{24}Al_{28}O_{64}]^{4+}(4e^-)$, *Adv. Mater.* **19**, 3564 (2007).
- [18] H. Hosono, J. Kim, Y. Toda, T. Kamiya, and S. Watanabe, Transparent amorphous oxide semiconductors for organic electronics: Application to inverted OLEDs, *Proc. Natl. Acad. Sci. USA* **114**, 233 (2017).
- [19] M. Kitano, Y. Inoue, Y. Yamazaki, F. Hayashi, S. Kanbara, S. Matsuishi, T. Yokoyama, S.-W. Kim, M. Hara, and H. Hosono, Ammonia synthesis using a stable electride as an electron donor and reversible hydrogen store, *Nat. Chem.* **4**, 934 (2012).
- [20] Y. Inoue, M. Kitano, K. Kishida, H. Abe, Y. Niwa, M. Sasase, Y. Fujita, H. Ishikawa, T. Yokoyama, M. Hara, and H. Hosono, Efficient and stable ammonia synthesis by self-organized flat Ru nanoparticles on calcium amide, *ACS Catal.* **6**, 7577 (2016).
- [21] Y. J. Kim, S. M. Kim, E. J. Cho, H. Hosono, J. W. Yang, and S. W. Kim, Two dimensional inorganic electride-promoted electron transfer efficiency in transfer hydrogenation of alkynes and alkenes, *Chem. Sci.* **6**, 3577 (2015).
- [22] I. R. Mokra and O. I. Bodak, Crystal structure of the CeScSi compound, *Dopov. Akad. Nauk Ukr. RSR, Ser. A* **4**, 312 (1979).
- [23] O. I. Bodak and Z. M. Kokhan, Ce-Sc-Ge system, *Inorg. Mater.* **19**, 987 (1984).
- [24] B. Chevalier, W. Hermes, B. Heying, U. C. Rodewald, A. Hammerschmidt, S. F. Matar, E. Gaudin, and R. Pöttgen, New hydrides $REScSiH$ and $REScGeH$ ($RE = La, Ce$): Structure, magnetism, and chemical bonding, *Chem. Mater.* **22**, 5013 (2010).
- [25] B. Chevalier, E. Gaudin, F. Weill, and J.-L. Bobet, Hydrogenation and physical properties of the ternary germanide CeCoGe: An anisotropic expansion of the unit cell, *Intermetallics* **12**, 437 (2004).
- [26] B. Chevalier and S. F. Matar, Effect of H insertion on the magnetic, electronic, and structural properties of CeCoSi, *Phys. Rev. B* **70**, 174408 (2004).
- [27] B. Chevalier, M. Pasturel, J.-L. Bobet, and O. Isnard, Influence of hydrogenation on the structural and magnetic properties of compounds based on cerium and crystallizing in the tetragonal CeFeSi-type structure, *Solid State Commun.* **134**, 529 (2005).

- [28] B. Chevalier, S. F. Matar, M. Ménétrier, J. S. Marcos, and J. R. Fernandez, Influence of Ce–H bonding on the physical properties of the hydrides CeCoSiH_{1.0} and CeCoGeH_{1.0}, *J. Phys.: Condens. Matter* **18**, 6045 (2006).
- [29] B. Chevalier, S. Matar, J. S. Marcos, and J. R. Fernandez, From antiferromagnetic ordering to spin fluctuation behavior induced by hydrogenation of ternary compounds CeCoSi and CeCoGe, *Phys. B: Condens. Matter* **378–380**, 795 (2006).
- [30] B. Chevalier, E. Gaudin, S. Tencé, B. Malaman, J. R. Fernandez, G. André, and B. Coqblin, Hydrogenation inducing antiferromagnetism in the heavy-fermion ternary silicide CeRuSi, *Phys. Rev. B* **77**, 014414 (2008).
- [31] S. Tencé, G. André, E. Gaudin, and B. Chevalier, Modulated magnetic structures of the antiferromagnetic hydride CeRuSiH, *J. Phys.: Condens. Matter* **20**, 255239 (2008).
- [32] B. Chevalier, S. Tencé, E. Gaudin, S. Matar, and J.-L. Bobet, Various magnetic behaviors of the hydrides deriving from the tetragonal CeFeSi-type compounds, *J. Alloys Compd.* **480**, 43 (2009).
- [33] J. Wu, Y. Gong, T. Inoshita, D. C. Fredrickson, J. Wang, Y. Lu, M. Kitano, and H. Hosono, Tiered electron anions in multiple voids of LaScSi and their applications to ammonia synthesis, *Adv. Mater.* **29**, 1700924 (2017).
- [34] D. C. Koskenmaki and K. A. Gschneidner, Cerium, in *Metals, Handbook on the Physics and Chemistry of Rare Earths Vol. 1* (Elsevier, Amsterdam, 1978), Chap. 4, pp. 337–377.
- [35] W. Kohn and L. J. Sham, Self-consistent equations including exchange and correlation effects, *Phys. Rev.* **140**, A1133 (1965).
- [36] P. Hohenberg and W. Kohn, Inhomogeneous electron gas, *Phys. Rev.* **136**, B864 (1964).
- [37] N. Lanatà, Y.-X. Yao, C.-Z. Wang, K.-M. Ho, and G. Kotliar, Interplay of spin-orbit and entropic effects in cerium, *Phys. Rev. B* **90**, 161104(R) (2014).
- [38] N. Lanatà, Y.-X. Yao, C.-Z. Wang, K.-M. Ho, J. Schmalian, K. Haule, and G. Kotliar, γ – α Isostructural Transition in Cerium, *Phys. Rev. Lett.* **111**, 196801 (2013).
- [39] M.-F. Tian, H.-F. Song, H.-F. Liu, C. Wang, Z. Fang, and X. Dai, Thermodynamics of the α – γ transition in cerium studied by an LDA+Gutzwiller method, *Phys. Rev. B* **91**, 125148 (2015).
- [40] M. Casadei, X. Ren, P. Rinke, A. Rubio, and M. Scheffler, Density-Functional Theory for *f*-Electron Systems: The α – γ Phase Transition in Cerium, *Phys. Rev. Lett.* **109**, 146402 (2012).
- [41] A. Georges, G. Kotliar, W. Krauth, and M. J. Rozenberg, Dynamical mean-field theory of strongly correlated fermion systems and the limit of infinite dimensions, *Rev. Mod. Phys.* **68**, 13 (1996).
- [42] K. Held, I. A. Nekrasov, G. Keller, V. Eyert, N. Blümer, A. K. McMahan, R. T. Scalettar, T. Pruschke, V. I. Anisimov, and D. Vollhardt, Realistic investigations of correlated electron systems with LDA+DMFT, *Phys. Status Solidi B* **243**, 2599 (2006).
- [43] G. Kotliar, S. Y. Savrasov, K. Haule, V. S. Oudovenko, O. Parcollet, and C. A. Marianetti, Electronic structure calculations with dynamical mean-field theory, *Rev. Mod. Phys.* **78**, 865 (2006).
- [44] J. Kuneš, A. V. Lukoyanov, V. I. Anisimov, R. T. Scalettar, and W. E. Pickett, Collapse of magnetic moment drives the Mott transition in MnO, *Nat. Mater.* **7**, 198 (2008).
- [45] I. Leonov, A. V. Ponomareva, R. Nazarov, and I. A. Abrikosov, Pressure-induced spin-state transition of iron in magnesiowüstite (Fe,Mg)O, *Phys. Rev. B* **96**, 075136 (2017).
- [46] A. A. Dyachenko, A. V. Lukoyanov, A. O. Shorikov, and V. I. Anisimov, Magnetically driven phase transitions with a large volume collapse in MnSe under pressure: A DFT+DMFT study, *Phys. Rev. B* **98**, 085139 (2018).
- [47] A. O. Shorikov, A. V. Lukoyanov, V. I. Anisimov, and S. Y. Savrasov, Pressure-driven metal-insulator transition in BiFeO₃ from dynamical mean-field theory, *Phys. Rev. B* **92**, 035125 (2015).
- [48] A. A. Dyachenko, A. O. Shorikov, A. V. Lukoyanov, and V. I. Anisimov, LDA+DMFT study of magnetic transition and metallization in CoO under pressure, *JETP Lett.* **96**, 56 (2012).
- [49] J. Kuneš, D. M. Korotin, M. A. Korotin, V. I. Anisimov, and P. Werner, Pressure-Driven Metal-Insulator Transition in Hematite from Dynamical Mean-Field Theory, *Phys. Rev. Lett.* **102**, 146402 (2009).
- [50] A. A. Dyachenko, A. O. Shorikov, A. V. Lukoyanov, and V. I. Anisimov, Two successive spin transitions in a wide range of pressure and coexistence of high- and low-spin states in clinoferrisilite FeSiO₃, *Phys. Rev. B* **93**, 245121 (2016).
- [51] A. V. Ushakov, A. O. Shorikov, V. I. Anisimov, N. V. Baranov, and S. V. Streltsov, Suppression of magnetism under pressure in FES: A DFT+DMFT study, *Phys. Rev. B* **95**, 205116 (2017).
- [52] M. B. Zöfl, I. A. Nekrasov, T. Pruschke, V. I. Anisimov, and J. Keller, Spectral and Magnetic Properties of α - and γ -Ce from Dynamical Mean-Field Theory and Local Density Approximation, *Phys. Rev. Lett.* **87**, 276403 (2001).
- [53] K. Held, A. K. McMahan, and R. T. Scalettar, Cerium Volume Collapse: Results from the Merger of Dynamical Mean-Field Theory and Local Density Approximation, *Phys. Rev. Lett.* **87**, 276404 (2001).
- [54] A. K. McMahan, K. Held, and R. T. Scalettar, Thermodynamic and spectral properties of compressed Ce calculated using a combined local-density approximation and dynamical mean-field theory, *Phys. Rev. B* **67**, 075108 (2003).
- [55] K. Haule, V. Oudovenko, S. Y. Savrasov, and G. Kotliar, The α \rightarrow γ Transition in Ce: A Theoretical View from Optical Spectroscopy, *Phys. Rev. Lett.* **94**, 036401 (2005).
- [56] B. Amadon, S. Biermann, A. Georges, and F. Aryasetiawan, The α – γ Transition of Cerium is Entropy Driven, *Phys. Rev. Lett.* **96**, 066402 (2006).
- [57] S. V. Streltsov, E. Gull, A. O. Shorikov, M. Troyer, V. I. Anisimov, and P. Werner, Magnetic susceptibility of cerium: An LDA+DMFT study, *Phys. Rev. B* **85**, 195109 (2012).
- [58] A. O. Shorikov, S. V. Streltsov, M. A. Korotin, and V. I. Anisimov, Phase stability of α -, γ -, and ϵ -Ce: DFT+DMFT study, *JETP Lett.* **102**, 616 (2015).
- [59] L. Huang and H. Lu, Electronic structure of cerium: A comprehensive first-principles study, *Phys. Rev. B* **99**, 045122 (2019).
- [60] M. S. Litsarev, I. Di Marco, P. Thunström, and O. Eriksson, Correlated electronic structure and chemical bonding of cerium pnictides and γ -Ce, *Phys. Rev. B* **86**, 115116 (2012).
- [61] M. Matsumoto, M. J. Han, J. Otsuki, and S. Y. Savrasov, First-Principles Simulations of Heavy Fermion Cerium Compounds Based on the Kondo Lattice, *Phys. Rev. Lett.* **103**, 096403 (2009).

- [62] H. Lu and L. Huang, Itinerant-localized crossover and orbital dependent correlations for $4f$ electrons in cerium-based ternary 122 compounds, *Phys. Rev. B* **98**, 195102 (2018).
- [63] J. P. Perdew, K. Burke, and M. Ernzerhof, Generalized Gradient Approximation Made Simple, *Phys. Rev. Lett.* **77**, 3865 (1996).
- [64] <http://elk.sourceforge.net/>.
- [65] G. H. Wannier, The structure of electronic excitation levels in insulating crystals, *Phys. Rev.* **52**, 191 (1937).
- [66] N. Marzari and D. Vanderbilt, Maximally localized generalized Wannier functions for composite energy bands, *Phys. Rev. B* **56**, 12847 (1997).
- [67] D. Korotin, A. V. Kozhevnikov, S. L. Skornyakov, I. Leonov, N. Binggeli, V. I. Anisimov, and G. Trimarchi, Construction and solution of a Wannier-functions based Hamiltonian in the pseudopotential plane-wave framework for strongly correlated materials, *Eur. Phys. J. B* **65**, 91 (2008).
- [68] B. Amadon, A self-consistent DFT+DMFT scheme in the projector augmented wave method: Applications to cerium, Ce_2O_3 and Pu_2O_3 with the Hubbard I solver and comparison to DFT+U, *J. Phys.: Condens. Matter* **24**, 075604 (2012).
- [69] K. Haule, C.-H. Yee, and K. Kim, Dynamical mean-field theory within the full-potential methods: Electronic structure of CeIrIn_5 , CeCoIn_5 , and CeRhIn_5 , *Phys. Rev. B* **81**, 195107 (2010).
- [70] M. Topsakal and R. Wentzcovitch, Accurate projected augmented wave (PAW) datasets for rare-earth elements (RE=La-Lu), *Comput. Mater. Sci.* **95**, 263 (2014).
- [71] B. Amadon, T. Applencourt, and F. Bruneval, Screened Coulomb interaction calculations: CRPA implementation and applications to dynamical screening and self-consistency in uranium dioxide and cerium, *Phys. Rev. B* **89**, 125110 (2014).
- [72] V. I. Anisimov, F. Aryasetiawan, and A. I. Lichtenstein, First-principles calculations of the electronic structure and spectra of strongly correlated systems: the LDA+U method, *J. Phys.: Condens. Matter* **9**, 767 (1997).
- [73] <http://www.amulet-code.org>.
- [74] P. Werner and A. J. Millis, Hybridization expansion impurity solver: General formulation and application to Kondo lattice and two-orbital models, *Phys. Rev. B* **74**, 155107 (2006).
- [75] A. Albuquerque, F. Alet, P. Corboz, P. Dayal, A. Feiguin, S. Fuchs, L. Gamper, E. Gull, S. Gürtler, A. Honecker, R. Igarashi, M. Körner, A. Kozhevnikov, A. Läuchli, S. Manmana, M. Matsumoto, I. McCulloch, F. Michel, R. Noack, G. Pawłowski *et al.*, The ALPS project release 1.3: Open-source software for strongly correlated systems, *J. Magn. Magn. Mater.* **310**, 1187 (2007).
- [76] K. S. D. Beach, R. J. Gooding, and F. Marsiglio, Reliable Padé analytical continuation method based on a high-accuracy symbolic computation algorithm, *Phys. Rev. B* **61**, 5147 (2000).
- [77] G. Pizzi, V. Vitale, R. Arita, S. Blügel, F. Freimuth, G. Géranton, M. Gibertini, D. Gresch, C. Johnson, T. Koretsune, J. Ibañez-Azpiroz, H. Lee, J.-M. Lihm, D. Marchand, A. Marrazzo, Y. Mokrousov, J. I. Mustafa, Y. Nohara, Y. Nomura, L. Paulatto *et al.*, WANNIER90 as a community code: New features and applications, *J. Phys.: Condens. Matter* **32**, 165902 (2020).
- [78] P. Giannozzi, S. Baroni, N. Bonini, M. Calandra, R. Car, C. Cavazzoni, D. Ceresoli, G. L. Chiarotti, M. Cococcioni, I. Dabo, A. D. Corso, S. de Gironcoli, S. Fabris, G. Fratesi, R. Gebauer, U. Gerstmann, C. Gougousis, A. Kokalj, M. Lazzeri, L. Martin-Samos *et al.*, QUANTUM ESPRESSO: A modular and open-source software project for quantum simulations of materials, *J. Phys.: Condens. Matter* **21**, 395502 (2009).
- [79] R. F. W. Bader, A quantum theory of molecular structure and its applications, *Chem. Rev.* **91**, 893 (1991).
- [80] G. Henkelman, A. Arnaldsson, and H. Jónsson, A fast and robust algorithm for Bader decomposition of charge density, *Comput. Mater. Sci.* **36**, 354 (2006).
- [81] K. Momma and F. Izumi, VESTA 3 for three-dimensional visualization of crystal, volumetric, and morphology data, *J. Appl. Crystallogr.* **44**, 1272 (2011).
- [82] See Supplemental Material at <http://link.aps.org/supplemental/10.1103/PhysRevB.105.085146> for details on methods and additional information, which includes Refs. [90,91].
- [83] A. D. Becke and K. E. Edgecombe, A simple measure of electron localization in atomic and molecular systems, *J. Chem. Phys.* **92**, 5397 (1990).
- [84] D. Y. Novoselov, D. M. Korotin, A. O. Shorikov, A. R. Oganov, and V. I. Anisimov, Interplay between the Coulomb interaction and hybridization in Ca and anomalous pressure dependence of the resistivity, *JETP Lett.* **109**, 387 (2019).
- [85] D. Y. Novoselov, V. I. Anisimov, and A. R. Oganov, Strong electronic correlations in interstitial magnetic centers of zero-dimensional electride $\beta\text{-Yb}_5\text{Sb}_3$, *Phys. Rev. B* **103**, 235126 (2021).
- [86] D. Y. Novoselov, D. M. Korotin, A. O. Shorikov, V. I. Anisimov, and A. R. Oganov, Interacting electrons in two-dimensional electride Ca_2N , *J. Phys. Chem. C* **125**, 15724 (2021).
- [87] D. I. Badrtdinov and S. A. Nikolaev, Localised magnetism in 2d electrides, *J. Mater. Chem. C* **8**, 7858 (2020).
- [88] S. G. Dale, A. O. de la Roza, and E. R. Johnson, Density-functional description of electrides, *Phys. Chem. Chem. Phys.* **16**, 14584 (2014).
- [89] Z. Li, J. Yang, J. G. Hou, and Q. Zhu, Is mayenite without clathrated oxygen an inorganic electride? *Angew. Chem., Int. Ed.* **43**, 6479 (2004).
- [90] P. E. Blöchl, Projector augmented-wave method, *Phys. Rev. B* **50**, 17953 (1994).
- [91] H. Hafermann, K. R. Patton, and P. Werner, Improved estimators for the self-energy and vertex function in hybridization-expansion continuous-time quantum monte carlo simulations, *Phys. Rev. B* **85**, 205106 (2012).